J Mol Model (2012) 18:4437–4446
DOI 10.1007/s00894-012-1441-0

ORIGINAL PAPER

Iterative experimental and virtual high-throughput screening identifies metabotropic glutamate receptor subtype 4 positive allosteric modulators

Ralf Mueller · Eric S. Dawson · Colleen M. Niswender · Mariusz Butkiewicz · Corey R. Hopkins · C. David Weaver · Craig W. Lindsley · P. Jeffrey Conn · Jens Meiler

Received: 9 February 2012 / Accepted: 18 April 2012 / Published online: 17 May 2012

Abstract Activation of metabotropic glutamate receptor subtype 4 has been shown to be efficacious in rodent models of Parkinson's disease. Artificial neural networks were trained based on a recently reported high throughput screen which identified 434 positive allosteric modulators of metabotropic glutamate receptor subtype 4 out of a set of approximately 155,000 compounds. A jury system containing three artificial neural networks achieved a theoretical enrichment of 15.4 when selecting the top 2 % compounds of an independent test dataset. The model was used to screen an external commercial database of approximately 450,000 drug-like compounds. 1,100 predicted active small molecules were tested experimentally using two distinct assays of $mGlu_4$ activity. This experiment yielded 67 positive allosteric modulators of metabotropic glutamate receptor subtype 4 that confirmed in both experimental systems. Compared to the 0.3 % active compounds in the primary screen, this constituted an enrichment of 22 fold.

Keywords Metabotropic glutamate receptor subtype 4 · Virtual high-throughput screening · Machine learning · Quantitative structure-activity relationship · Enrichment

R. Mueller · M. Butkiewicz · C. R. Hopkins · C. W. Lindsley · J. Meiler
Department of Chemistry, Vanderbilt University, Nashville, TN 37232-6600, USA

R. Mueller · E. S. Dawson · C. M. Niswender · C. R. Hopkins · C. D. Weaver · C. W. Lindsley · P. J. Conn · J. Meiler
Department of Pharmacology, Vanderbilt University, Nashville, TN 37232-6600, USA

C. D. Weaver · C. W. Lindsley · P. J. Conn · J. Meiler
Institute for Chemical Biology, Vanderbilt University, Nashville, TN 37232-6600, USA

J. Meiler (✉)
Center for Structural Biology, Vanderbilt University, Nashville, TN 37232-6600, USA
e-mail: jens.meiler@vanderbilt.edu
URL: www.meilerlab.org

E. S. Dawson · C. M. Niswender · C. R. Hopkins · C. W. Lindsley · P. J. Conn
Center for Neuroscience Drug Discovery, Vanderbilt University, Nashville, TN 37232-6600, USA

Introduction

This study implements a machine learning approach (Artificial Neural Networks, ANNs) to virtually screen commercially available compounds for positive allosteric modulators (PAMs) of metabotropic glutamate receptor subtype 4 ($mGlu_4$). Marino and Conn [1, 2] showed that activation of $mGlu_4$ is a viable option in treating Parkinson's disease (PD), a debilitating movement disorder that afflicts more than 1 million people in North America. In Parkinson's patients, there is a decrease in GABAergic transmission at the inhibitory striatopallidal synapse within the basal ganglia; this abnormality is thought to contribute to the motor dysfunctions observed in PD patients. Current PD treatments that are focused on dopamine-replacement strategies ultimately fail in most patients because of loss of efficacy and severe adverse effects that worsen as the disease progresses [2, 3]. Selective activation of $mGlu_4$ could provide palliative benefit in PD. Further, selectively targeting $mGlu_4$ avoids the loss of efficacy and severe side-effects of long-term dopamine replacement therapy. In 2003 Maj [2, 4] et al. reported on the discovery of (−)-PHCCC, the

first positive allosteric modulator of $mGlu_4$ with demonstrated selectivity for group III mGlus, but also a partial antagonist for $mGlu_1$ (group I). Around the same time, Mathiesen [5] et al. showed that SIB-1893 and MPEP (a known $mGlu_5$ antagonist [6]) are $mGlu_4$ PAMs.

Despite the success of many GPCR-based drug discovery programs, many of the developed ligands lack selectivity. The traditional approach to target the endogenous ligand (orthosteric)-binding site has suffered from a paucity of suitably subtype-selective ligands as orthosteric binding sites are highly conserved between GPCR subtypes. An alternative approach is to target allosteric sites that are topographically distinct from the orthosteric site, either enhancing or inhibiting receptor activation [7]. Discovery and characterization of allosteric modulators of GPCRs has gained significant momentum over the last few years, especially since the clinical validity of GPCR allosteric modulators was demonstrated with two allosteric modulators entering the market [8, 9]. Thus, allosteric modulation represents an exciting novel means of targeting GPCRs particularly for CNS disorders, a therapeutic area with one of the highest rates of attrition in drug discovery [10].

Recently, Niswender [11] et al. reported the discovery of 434 PAMs of $mGlu_4$ from a high-throughput screen of approximately 155,000 compounds. The study highlighted a series of cyclohexyl amides joined to a substituted phenyl ring. The structures of these tested molecules and their experimentally determined EC_{50} towards $mGlu_4$ potentiation were employed in the ANNs described in this paper. Engers et al. [12] discuss the synthesis and evaluation of a set of heterobiarylamides optimized for penetrating the central nervous system. Around the same time, several pyrazolo[3,4-d]pyrimidines were also described to be novel $mGlu_4$ positive allosteric modulators [13]. Two challenges in further developing PAMs of $mGlu_4$ as a PD treatment strategy are the low hit-rate of 0.3 % in the original high-throughput screen resulting in a small number of available ligands and the 'flat' structure activity relationship (SAR) around the 'proof of concept' compound PHCCC. Even slight structural modifications lead to complete loss of activity for the reported compounds [14]. However, successful modifications of PHCCC were reported later by our group [15]. The present study addressed both challenges by identifying additional PAMs from commercially available compound libraries and exploring the chemical space around the known active compounds.

Quantitative structure activity relationship (QSAR) models describe the often complex, non-linear relation between the chemical and physical properties of molecules and their biological activity; for a review of different methods see Todeschini et al. [16, 17]. Classical QSAR was introduced by Hansch et al. by deriving biological activity from electron density [18]. In 1988 Cramer [19] introduced Comparative Molecular Field Analysis (CoMFA.) CoMFA establishes 3D-QSAR by correlating sterics and electrostatics to the bioactivity data. This approach was expanded into the Comparative Molecular Similarity Index Analysis (CoMSIA) by Klebe [20] in 1994. However, both approaches rely on the spatial alignment of small molecules sharing a common scaffold. The QSAR techniques employed in the present and similar studies utilize 2D molecular fingerprints and 3D molecular descriptors coupled with machine learning [21–23]. These descriptors are independent from the orientation of the small molecule and the existence of a common scaffold. ANNs have been successfully applied in biochemistry to generate QSAR models [23–27]. Our group recently published a theoretical comparison of machine learning techniques for identification of compounds that are predicted allosteric modulators of the $mGlu_5$ glutamate response [28, 29].

In the present study, artificial neural networks (ANNs) were trained on descriptors computed with the software package ADRIANA [30] linking chemical properties of small molecules to their potency as PAMs of $mGlu_4$. Fragment-independent scalar descriptors, 2D and 3D surface and auto-correlation functions, and radial distribution functions are employed to encode a large diversity of chemotypes into comparable mathematical representations [29].

Methods

Two independent assays for primary and confirmatory screen

The compounds identified in the virtual screen were ordered from ChemBridge and tested at the Vanderbilt HTS facility. These compounds were screened in single point at a nominal 10 μM concentration employing the human $mGlu_4/G_{qi5}$ calcium mobilization assay as well as the rat $mGlu_4$ thallium flux assay described in Niswender et al. [11, 31]. Compounds exceeding three standard deviations over the control EC_{20} response were then screened in concentration-response curve format in both assays.

Preparing the input for the ANNs

Only 0.3 % (432 molecules) of the whole data set (156,146 molecules) was active. For training, the dataset was oversampled by a factor of 360 (see Fig. 1) [29]. This leads to a data set with 311,234 molecules where approximately half of the data points were active and the other half inactive.

Three-dimensional models of all 156,146 molecules from the original HTS were generated using CORINA [32]. These models served as input for the ADRIANA [33]

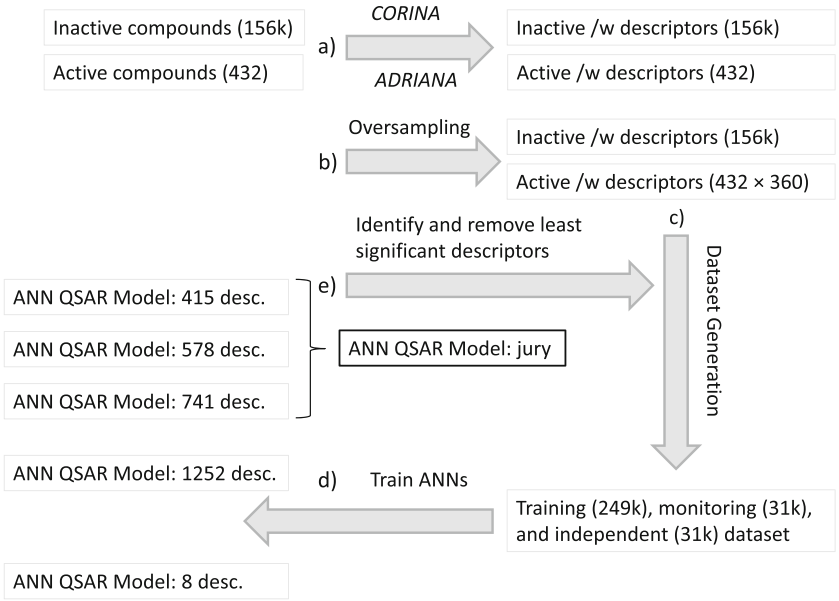

Fig. 1 Overall model generation workflow: **a** SD files were provided with active and inactive compounds towards $mGlu_4$ determined by HTS and CRC; CORINA and ADRIANA were employed to generate 3D structures and molecular descriptors; **b** active molecules were oversampled 360 times to balance data sets; **c** molecules were randomly distributed between training (80 %), monitoring (10 %), and independent (10 %) datasets; **d** ANNs were trained and **e** low sensitivity descriptors were removed until the quality measures (see Table 2) no longer improved; the best three ANNs were combined into a jury network

software package. All 35 categories (scalar, 2D/3D auto-correlation, RDF (eight each), surface auto-correlation (three), see Table 1) were computed implementing the default values in each category. Approximately 4 % of all molecules were not properly encoded by ADRIANA and removed from the data set. The final data set consisted of 298,914 data points.

Training the ANN on the logarithm of the half maximal effective concentration EC_{50}

The experimentally determined EC_{50} values of the active compounds ranged from 0.4 μM to 15.8 μM. To distinguish between active and inactive compounds, all inactive compounds were set to an arbitrary potency of 1 mM. The output for training the ANN consisted of the natural logarithm of the $ln(EC_{50})$ values ranging from −14.7 (most active) over −11.1 (least active) to −6.9 (inactive). The *root mean square deviation (rmsd)* between experimental and predicted EC_{50} values was employed as objective function in training the ANNs:

$$rmsd = \sqrt{\frac{\sum_{i=1}^{n} (exp_i - pred_i)^2}{n}} \quad (1)$$

where exp_i is the experimentally determined $ln(EC_{50})$ value and $pred_i$ the predicted $ln(EC_{50})$ value.

From the 298,914 data points in the oversampled data set, 239,132 (80 %) were employed in the actual training of the ANN. The monitoring data set consisted of 29,891 data points (10 %). The *rmsd* between experimental and predicted $ln(EC_{50})$ was computed for the monitoring data set after each iteration over the full training data set. Once the *rmsd* was minimized, the training was terminated, and the *rmsd* of the remaining 10 % (independent data set) computed (see Table 2). Care was taken to exclude overlap between training, monitor, and independent data set.

Overall structure of the ANNs and the jury system

The trained ANNs consisted of the input layer with up to 1,252 chemical descriptors, the hidden layer consisting of eight neurons, and one neuron in the output layer predicting the $ln(EC_{50})$ of the described molecule. The sigmoid function $S(x) = 1/(1 + exp(-x))$served as activation function of the neurons. The ANNs were trained by implementing resilient back-propagation of errors [34], a supervised learning approach. The training was terminated after up to 40,000 iterations when the monitoring dataset achieved its minimum *rmsd*. It took up to 13 hours per network using eight cores of a core2 quad 2.33 GHz Intel Xeon microprocessor in parallel on the 64-bit version of Red Hat Enterprise Linux 5.2.

The outputs of the three best ANNs were used as input for a jury ANN that consisted of three inputs, four hidden neurons, and one output (Fig. 2). The training of the jury ANN terminated after 290 steps.

Selection of the optimal set of descriptors of chemical structure

It is crucial to select the optimal set of descriptors from the 35 available categories. In a top-down approach, the least significant categories for predicting $ln(EC_{50})$ were successively removed to increase the predictive power of the according ANNs. The advantage lies in removing degrees of freedom from the ANN by reducing the number of inputs. Since the number of data points stays the same, the signal-

Table 1 Summary of 1,252 molecular descriptors in 35 categories computed with *ADRIANA*

	Description Method	Description Property	Abbreviation	Number
1	Scalar descriptors	Molecular weight of compound	Weight	1
2		Number of hydrogen bonding acceptors	HDon	1
3		Number of hydrogen bonding donors	HAcc	1
4		Octanol/water partition coefficient in [log units]	XlogP	1
5		Topological polar surface area in [Å^2]	TPSA	1
6		Mean molecular polarizability in [Å^3]	Polariz	1
7		Dipole moment in [Debye]	Dipol	1
8		Solubility of the molecule in water in [log units]	LogS	1
9	2D Autocorrelation	atom identities	2DA_Ident	11
10		σ atom charges	2DA_SigChg	11
11		π atom charges	2DA_PiChg	11
12		total charges	2DA_TotChg	11
13		σ atom electronegativities	2DA_SigEN	11
14		π atom electronegativities	2DA_PiEN	11
15		lone pair electronegativities	2DA_LpEN	11
16		effective atom polarizabilities	2DA_Polariz	11
17	3D Autocorrelation	atom identities	3DA_Ident	12
18		σ atom charges	3DA_SigChg	12
19		π atom charges	3DA_PiChg	12
20		total charges	3DA_TotChg	12
21		σ atom electronegativities	3DA_SigEN	12
22		π atom electronegativities	3DA_PiEN	12
23		lone pair electronegativities	3DA_LpEN	12
24		effective atom polarizabilities	3DA_Polariz	12
25	Radial Distribution Function	atom identities	RDF_Ident	128
26		σ atom charges	RDF_SigChg	128
27		π atom charges	RDF_PiChg	128
28		total charges	RDF_TotChg	128
29		σ atom electronegativities	RDF_SigEN	128
30		π atom electronegativities	RDF_PiEN	128
31		lone pair electronegativities	RDF_LpEN	128
32		effective atom polarizabilities	RDF_Polariz	128
33	Surface Autocorrelation	molecular electrostatic potential	Surf_ESP	12
34		hydrogen bonding potential	Surf_HBP	12
35		hydrophobicity potential	Surf_HPP	12
Total				1252

Table 2 QSAR: *rmsd*, *auc*, and enrichment values per model

Iteration	Number and type of descriptors		train	*rmsd* monitor	independent	*auc*	enrichment at 2 %
all	1252	1–35	0.204	0.232	0.234	0.708	7.3
scalar	8	1–8	0.232	0.236	0.239	0.631	1.2
1	741	1–8, 14–16, 21–23, 25, 29–33, 35	0.224	0.224	0.227	0.703	7.1
2	578	1–8, 15–16, 23, 25, 30 – 33, 35	0.187	0.212	0.229	0.706	13.0
3	415	1–8, 15, 25, 30–31, 35	0.192	0.211	0.222	0.804	10.7
jury	–	–	0.159	0.214	0.207	0.732	15.4

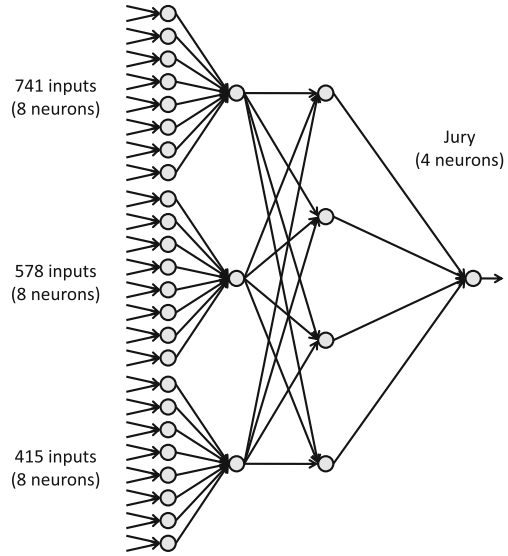

Fig. 2 Schematic view of the jury system: The output of the best three ANNs according to the quality measures reported in Table 2 were employed as inputs for a jury ANN with four hidden neurons

to-noise ratio improves. This procedure is described in detail elsewhere [29].

The input sensitivity of each of the 27 non-scalar descriptor categories was determined as norm over the individual input sensitivity values within this category. The descriptor categories were sorted by input sensitivity. In each step, categories comprising the least 10 % of input sensitivity were removed. This process was repeated until the quality measures were optimized (see Table 2).

Enrichment and area under the curve complement *rmsd* as quality measures

Analysis of the *rmsd* proved to be a poor indicator for model quality (see Table 2). Hence, all models were also assessed in terms of their binary classification power using enrichment and area under the curve (*auc*) quality measures. Receiver operating characteristic (ROC) curves were generated as a measure to evaluate predictive power of the machine learning approaches. ROC curves plot the rate of true positives *TP/P* versus the rate of false positives *FP/N* of a binary classifier, here biological activity (see Figs. 3 and 4). *TP* and *FP* represent the numbers of known active and inactive compounds within a given subset of small molecules ordered by their predicted biological activity. Similarly, *P* and *N* represent the according numbers for the whole HTS dataset. The diagonal represents the performance expected from a random predictor. A higher *auc* of a ROC curve represents a better predictive power of the according model.

The enrichment represents the expected factor by which the fraction of active compounds is increased in a small set of compounds resulting from an *in silico* virtual screen

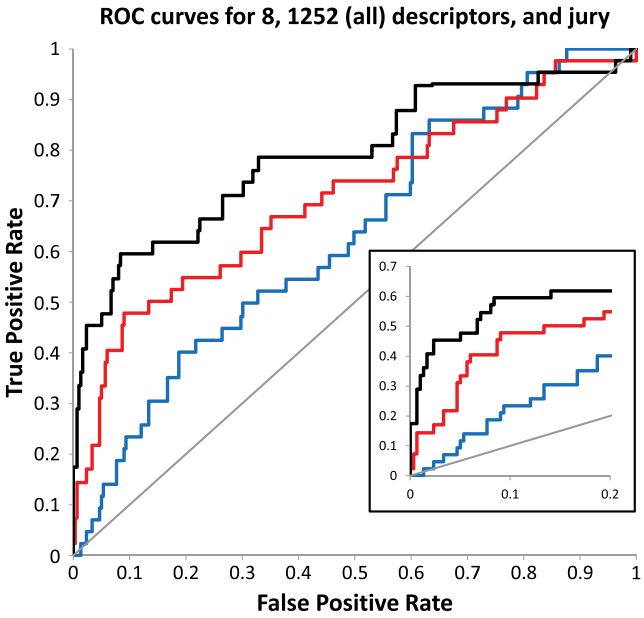

Fig. 3 Receiver Operating Characteristic (ROC) curve plot for classical (blue), all (red), and jury (black) approach: This plot compares classical QSAR (eight scalar descriptors) with utilizing all (1,252) available ADRIANA descriptors and a jury approach. It demonstrates that ADRIANA descriptors add to the classical approach and that a jury approach improves performance even further. The inset shows the first 20 % of the False Positive rate

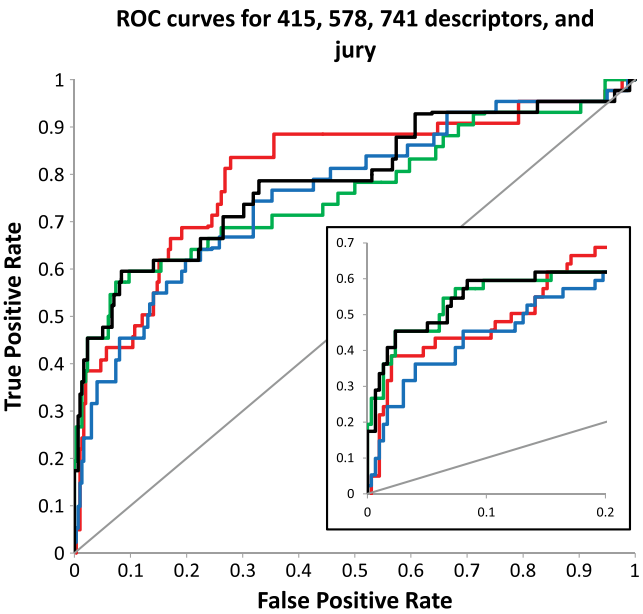

Fig. 4 Receiver Operating Characteristic (ROC) curve plot for 415 (red), 578 (green), 741 (blue), and jury (black) approach: The three optimized descriptor sets (415, 578, 741) perform similarly well as the jury approach. However, the jury approach is more stable compared to the three other ANNs, as can be seen in Table 2. The inset shows the first 20 % of the False Positive rate

compared to the same fraction in the original HTS dataset (0.28 %).

$$enrichment = \frac{TP}{TP + FP} \Big/ \frac{P}{P + N} \quad (2)$$

where P represents the total number of active compounds (positives) in the training dataset and N the total number of inactive compounds (negatives). TP stands for true positives – active compounds found in a compound library from virtual screening. FP are false positives – compounds predicted to be active that turn out to be inactive. Enrichments can be determined when experimentally testing a compound library obtained from a virtual screen or for an independent dataset set aside during training of the QSAR method. The enrichments reported in Table 2 were determined when selecting 2 % of the compounds in the independent dataset predicted to be most active.

Implementation

The ANN and the Resilient Propagation training algorithm [34] were implemented in the BioChemistryLibrary (BCL). The BCL is an in house developed, object-oriented library written in the C++ programming language currently consisting of approximately 400 classes and 300,000 lines of code. Chemical descriptors were computed with ADRIANA [30, 33] based on three-dimensional structures generated by CORINA [32].

Results

Artificial Neural Networks (ANNs) were trained to predict the capability of drug-like molecules for allosteric potentiation of the metabotropic glutamate receptor subtype 4 ($mGlu_4$) based on a High Throughput Screen (HTS) as reported by Niswender et al. [11]. Commercially available databases of small molecules were virtually screened for novel PAMs of $mGlu_4$. Hit compounds were verified experimentally in a human $mGlu_4$ G_{qi5}-mediated calcium assay and a rat $mGlu_4$ thallium flux assay.

Optimization of molecular descriptor set improves prediction results

An ANN was trained using only the scalar descriptors 1–8 to report a baseline performance using only naïve descriptors (Fig. 3 and Table 2) yielding an *auc* value of 0.631. The enrichment equals 1.2 at a compound cutoff of 2 %. The relative *rmsd* value for the independent data set is 0.238. 'Total Polarizable Surface Area' was the input with the highest sensitivity (0.87) in this model with the other descriptor sensitivities ranging from 0.07 ('Dipole Moment') to 0.48 ('Hydrogen Bond Acceptors'). The second baseline model involved all 1,252 descriptors as inputs. The *auc* and enrichment values improved to 0.708 and 7.3, respectively, while the *rmsd* dropped to 0.234.

In a 1st round of descriptor optimization, one third of the descriptor categories with the lowest input sensitivity were removed. Note that the scalar descriptors were kept in all models to facilitate comparison of input sensitivities with the baseline. This procedure leads to a final model containing 741 descriptors in 21 categories (see Table 2) without a significant change in model quality (*auc*: 0.703, *rmsd*: 0.227, enrichment: 7.1). The 2nd round yielded a model with 578 descriptors in 17 categories. The quality measures were better than the model with all descriptors with an *auc* of 0.706, *rmsd* of 0.229, and an improved enrichment of 13.0. The last iteration left 415 descriptors in 13 categories. While the *auc* value (0.804) and *rmsd* value (0.222) improved, the enrichment (10.7) dropped.

Jury model combines favorable features of all previous models

As these QSAR models have a comparable quality and enrichment values are affiliated with high uncertainties, a jury approach was tested to combine models. An ANN was trained on the output of the three ANNs with the reduced descriptor sets (see Fig. 2). This procedure improved the critical enrichment value to 15.4 and reduced the *rmsd* to 0.207. The *auc* value is with 0.732, a value lower than the 0.804 value reported for the ANN model with 415 descriptors. However, the reduced *auc* value this model results from the second half of the ROC curve, which is not employed when predicting molecules with high activities (Fig. 4).

Virtual screening of ChemBridge compound library

The ANN QSAR model was applied in a virtual screen of the ChemBridge EXPRESS-Pick collection of commercially available compounds. *In silico* screening of the entire library of ~450,000 compounds took approximately ten hours on a regular personal computer. A total of 1,108 compounds with predicted EC_{50} values below 3 μM for $mGlu_4$ PAM activity were selected.

Screening these compounds in the human $mGlu_4/G_{qi5}$ calcium mobilization assay as well as the rat $mGlu_4$ thallium flux assay described in Niswender et al. [11, 31] identified 168 primary hits which were then moved to screening in concentration-response curve format in both assays. 67 compounds were confirmed as potentiators in both assays, representing an enrichment of 67/1,108×156,184/434=22 relative to the initial experimental HTS hit rate. The experimentally observed enrichment is consistent with the enrichment values predicted from analysis of an independent

dataset during development of the QSAR model, given the large uncertainty of these values (Table 2).

The EC_{50} of the 67 confirmed potentiators ranged from 0.4 μM to 15.8 μM with three compounds below 1 μM in the human G_{qi5} assay and from 0.4 μM to >10 μM with three compounds below 1 μM in the rat thallium flux assay.

Simple similarity search fails to identify 54 out of 67 confirmed potentiators

To compare the ANN virtual screen with a more naïve similarity search, we selected 1,116 small molecules from the ChemBridge database based on MACCS structural key fingerprint similarity to known actives. The number of compounds was chosen to create a dataset of similar size to the one selected through the ANN. The artificially high Tanimoto coefficient cutoff of 96.7 % indicates that a similarity search with a reasonable Tanimoto coefficient would create a dataset much too large for experimental verification. The intersection between this set of 1,116 compounds and the 67 potentiators identified by the ANN contains 13 compounds (19 %) missing 54 compounds identified by the ANN virtual HTS.

Enrichment of 22 in known benzo-oxazoles scaffold

The rate of PAMs from the benzo-oxazole scaffold in the original HTS constituted 88 out of 26,180 (0.34 %, MOE [35] similarity search employing MACCS fingerprints at 85 % Tanimoto Superset/Subset.) A simple similarity search for benzo-oxazoles would preserve this rate while the virtual HTS enriched benzo-oxazoles by a factor of 8/133*156,146/432=22.

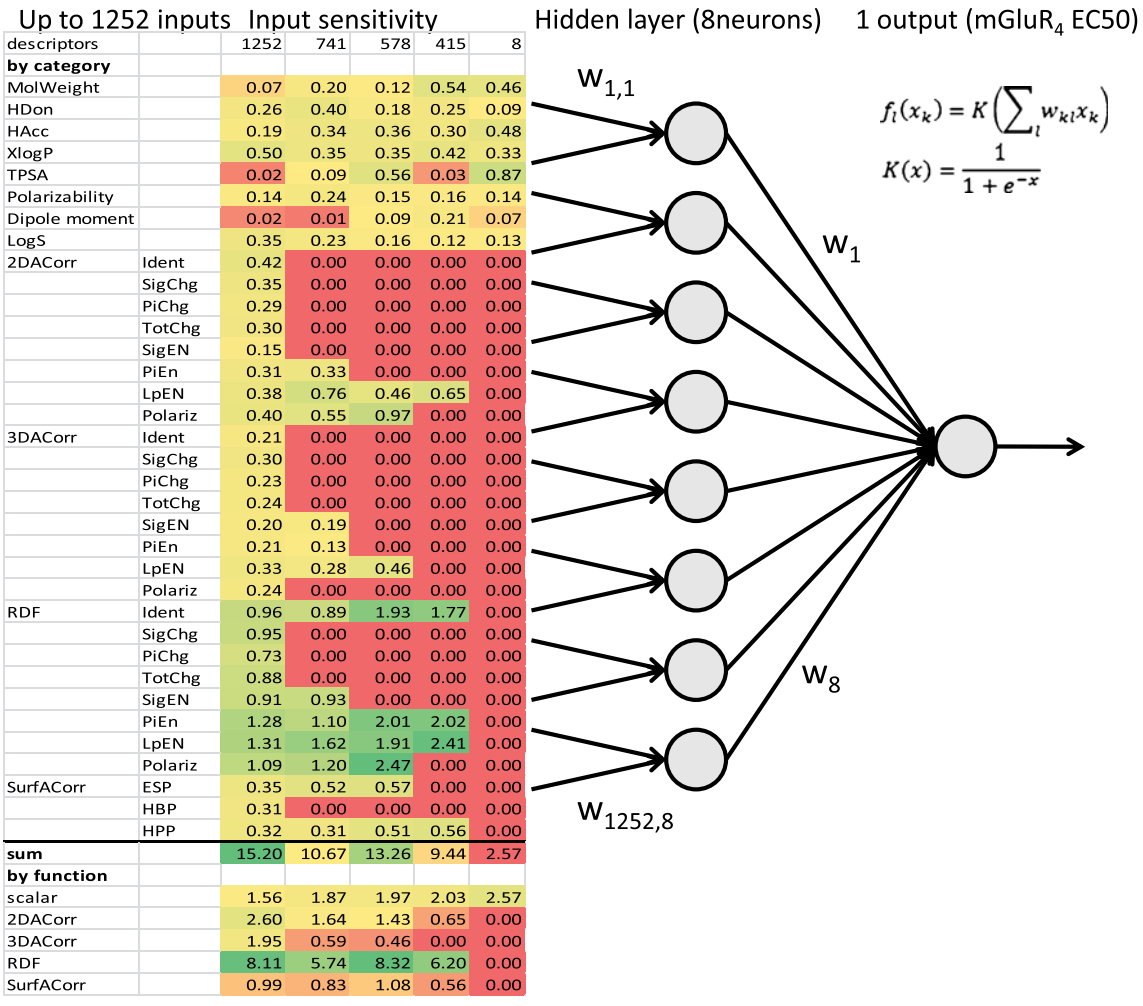

descriptors		1252	741	578	415	8
by category						
MolWeight		0.07	0.20	0.12	0.54	0.46
HDon		0.26	0.40	0.18	0.25	0.09
HAcc		0.19	0.34	0.36	0.30	0.48
XlogP		0.50	0.35	0.35	0.42	0.33
TPSA		0.02	0.09	0.56	0.03	0.87
Polarizability		0.14	0.24	0.15	0.16	0.14
Dipole moment		0.02	0.01	0.09	0.21	0.07
LogS		0.35	0.23	0.16	0.12	0.13
2DACorr	Ident	0.42	0.00	0.00	0.00	0.00
	SigChg	0.35	0.00	0.00	0.00	0.00
	PiChg	0.29	0.00	0.00	0.00	0.00
	TotChg	0.30	0.00	0.00	0.00	0.00
	SigEN	0.15	0.00	0.00	0.00	0.00
	PiEn	0.31	0.33	0.00	0.00	0.00
	LpEN	0.38	0.76	0.46	0.65	0.00
	Polariz	0.40	0.55	0.97	0.00	0.00
3DACorr	Ident	0.21	0.00	0.00	0.00	0.00
	SigChg	0.30	0.00	0.00	0.00	0.00
	PiChg	0.23	0.00	0.00	0.00	0.00
	TotChg	0.24	0.00	0.00	0.00	0.00
	SigEN	0.20	0.19	0.00	0.00	0.00
	PiEn	0.21	0.13	0.00	0.00	0.00
	LpEN	0.33	0.28	0.46	0.00	0.00
	Polariz	0.24	0.00	0.00	0.00	0.00
RDF	Ident	0.96	0.89	1.93	1.77	0.00
	SigChg	0.95	0.00	0.00	0.00	0.00
	PiChg	0.73	0.00	0.00	0.00	0.00
	TotChg	0.88	0.00	0.00	0.00	0.00
	SigEN	0.91	0.93	0.00	0.00	0.00
	PiEn	1.28	1.10	2.01	2.02	0.00
	LpEN	1.31	1.62	1.91	2.41	0.00
	Polariz	1.09	1.20	2.47	0.00	0.00
SurfACorr	ESP	0.35	0.52	0.57	0.00	0.00
	HBP	0.31	0.00	0.00	0.00	0.00
	HPP	0.32	0.31	0.51	0.56	0.00
sum		15.20	10.67	13.26	9.44	2.57
by function						
scalar		1.56	1.87	1.97	2.03	2.57
2DACorr		2.60	1.64	1.43	0.65	0.00
3DACorr		1.95	0.59	0.46	0.00	0.00
RDF		8.11	5.74	8.32	6.20	0.00
SurfACorr		0.99	0.83	1.08	0.56	0.00

Fig. 5 Schematic view of an ANN: The input to the ANN consists of up to 1,252 descriptors in 35 categories. The weighted sum of the inputs is propagated through the activation function and fed into the hidden layer (8 neurons). The output is the predicted value of the logarithm of the EC_{50} of the small molecule towards potentiation of glutamate response at the metabotropic glutamate receptor 4. The heat map shows the input sensitivity of each category from lowest (red) to highest (green)

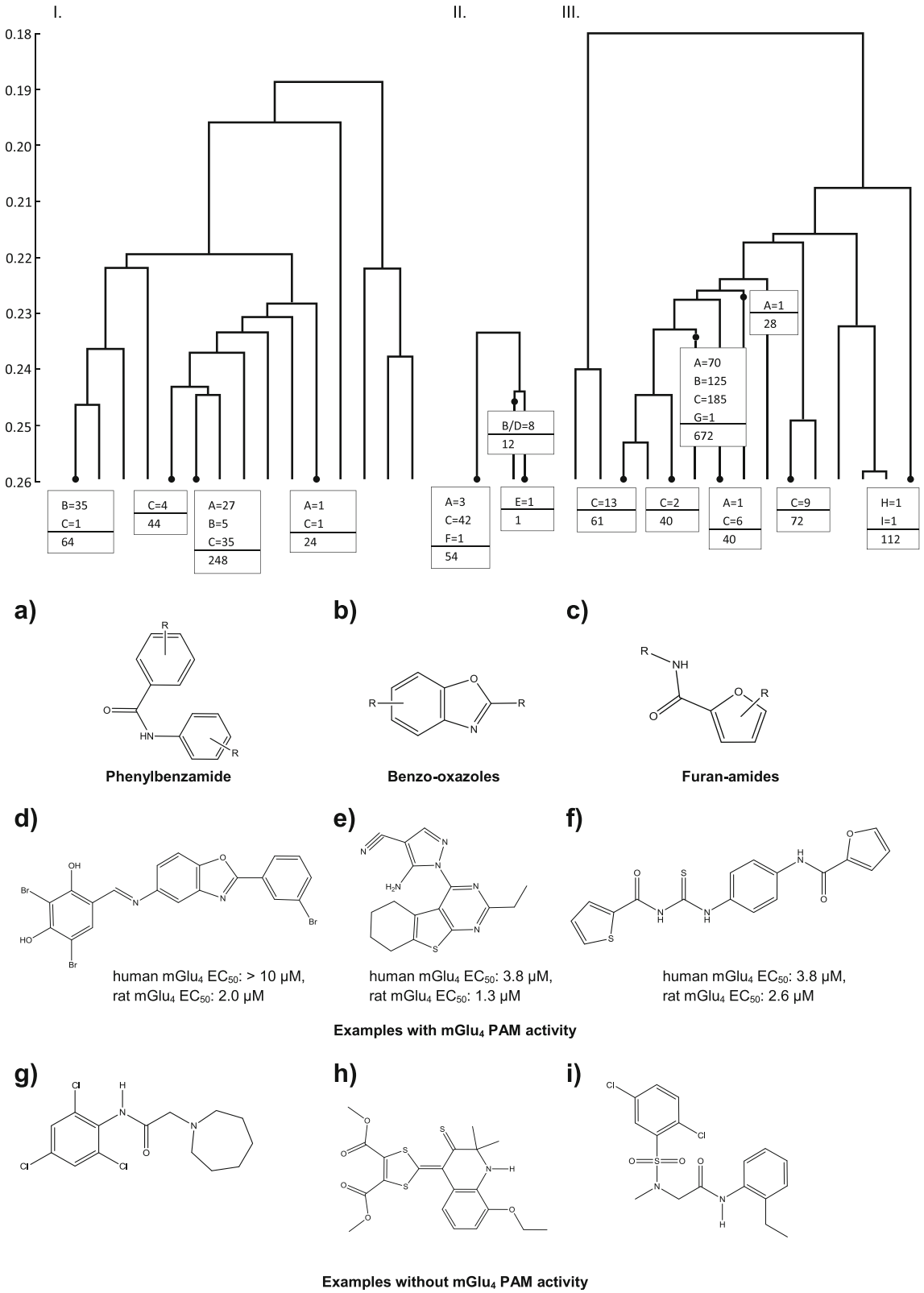

Fig. 6 Scaffold category analysis: (**I**) Scaffold composition of 432 $mGlu_4$ PAMs from HTS. $mGlu_4$ PAMs were clustered with the Mathematica package using the Tanimoto coefficient of the largest common substructure as distance measure. Three major scaffolds are constituted by 28 phenylbenzamides (6.5 %, a), 40 benzo-oxazoles (9.3 %, b), and 41 (9.5 %, c) furan-amides. (**II**) Scaffold composition of 67 active compounds in the postscreen. (**III**) Scaffold composition of inactive compounds in the postscreen. Compounds d, e, and f are examples for active compounds identified by the virtual HTS, where g, h, and i were found to be inactive

Discussion

Radial Distribution Functions (RDFs) are most important descriptors for predicting $mGlu_4$ PAM activity

Several of the descriptor categories (see Table 1) employ the same chemical property but different encoding functions (2D vs. 3D auto-correlation and Radial Distribution Functions). Therefore, a descriptor optimization strategy was critical to identify the smallest set of descriptors needed for optimal QSAR models. Using this technique, the number of parameters (weights) in the ANNs is reduced, improving the signal-to-noise ratio for the trained models. To determine the 'least necessary' descriptor categories, the input sensitivity (see Methods) of each input with respect to the output of the ANN, i.e. biological activity prediction, was determined.

As more descriptors are removed from the inputs, the input sensitivity values increase for RDFs (see Fig. 5). Specifically, RDFs for π- and lone pair electronegativity play an important role. RDFs for identity and polarizability are featured most prominently in the model with 578 descriptors which is the best non-jury network (see Table 2). The importance of these descriptors immediately makes sense, since the active compounds of the original High Throughput Screening often feature phenyl rings and amide substructures that are well described by such RDFs.

Virtual screening yields active compounds similar to known hits

The 67 newly identified $mGlu_4$ PAM compounds contained eight benzo-oxazoles, 42 furan-amides including 22 thioureas, and three phenylbenzamides. All three compound classes were represented in the original HTS hits [11, 36, 37] and featured modifications in R-groups (Fig. 6). Experimentally inactive compounds from these classes included 72 phenylbenzamides, 125 benzo-oxazoles, and 215 furanamides out of 1,041 inactive compounds.

Conformational ensembles could improve activity prediction from 3D molecular descriptors

CORINA provides one low energy conformation per small molecule. For flexible molecules multiple conformations of similar energy can exist. The conformation of the small molecule binding allosterically to the $mGlu_4$ is then unknown. This shortcoming of the present approach could be addressed by generating an ensemble of low energy conformations for each small molecule and using the lowest predicted EC_{50} value in virtual screening. The molecular libraries employed in the present study are dominated by rather rigid molecules with few rotatable bonds. Therefore we speculate that the impact of additional conformational sampling is small.

Conclusions

Artificial Neural Networks were trained to generate QSAR models from an HTS experimental dataset of compounds with $hmGlu_4$ G_{qi5} assay activity. A jury system, based on the three ANN models, generated improved enrichments when compared to each individual model. The enrichment factor of 22 determined from biological testing of 1,100 compounds prioritized from a commercial library of ~450,000 substances demonstrates the predictive power of the method.

References

1. Marino MJ, Conn PJ (2006) Glutamate-based therapeutic approaches: allosteric modulators of metabotropic glutamate receptors. Curr Opin Pharmacol 6(1):98–102. doi:10.1016/j.coph.2005.09.006
2. Marino MJ, Williams DL, O'Brien JA, Valenti O, McDonald TP, Clements MK, Wang R, DiLella AG, Hess JF, Kinney GG, Conn PJ (2003) Allosteric modulation of group III metabotropic glutamate receptor 4: a potential approach to Parkinson's disease treatment. Proc Natl Acad Sci USA 100(23):13668–13673. doi:10.1073/pnas.1835724100
3. Marino M, Valenti O, Conn PJ (2003) Glutamate receptors and Parkinson's disease: opportunities for intervention. Drugs Aging 20(5):377–397
4. Maj M, Bruno V, Dragic Z, Yamamoto R, Battaglia G, Inderbitzin W, Stoehr N, Stein T, Gasparini F, Vranesic I, Kuhn R, Nicoletti F, Flor PJ (2003) (−)-PHCCC, a positive allosteric modulator of mGluR4: characterization, mechanism of action, and neuroprotection. Neuropharmacol 45(7):895–906. doi:10.1016/s0028-3908(03)00271-5
5. Mathiesen JM, Svendsen N, Bräuner-Osborne H, Thomsen C, Ramirez MT (2003) Positive allosteric modulation of the human metabotropic glutamate receptor 4 (hmGluR4) by SIB-1893 and MPEP. Br J Pharmacol 138(6):1026–1030. doi:10.1038/sj.bjp.0705159
6. Gasparini F, Lingenhöhl K, Stoehr N, Flor PJ, Heinrich M, Vranesic I, Biollaz M, Allgeier H, Heckendorn R, Urwyler S, Varney MA, Johnson EC, Hess SD, Rao SP, Sacaan AI, Santori EM, Veliçelebi G, Kuhn R (1999) 2-Methyl-6-(phenylethynyl)-pyridine (MPEP), a potent, selective and systemically active mGlu5 receptor antagonist. Neuropharmacol 38 (10):1493–1503. doi:10.1016/s0028-3908(99)00082-9
7. Gregory KJ, Dong EN, Meiler J, Conn PJ (2010) Allosteric Modulation of Metabotropic Glutamate Receptors: Structural Insights and Therapeutic Potential. Neuropharmacology. doi:10.1016/j.neuropharm.2010.07.007
8. Lindberg JS, Culleton B, Wong G, Borah MF, Clark RV, Shapiro WB, Roger SD, Husserl FE, Klassen PS, Guo MD, Albizem MB, Coburn JW (2005) Cinacalcet HCl, an oral calcimimetic agent for the treatment of secondary hyperparathyroidism in hemodialysis and peritoneal dialysis: a randomized, double-blind, multicenter study. J Am Soc Nephrol 16(3):800–807. doi:10.1681/asn.2004060512
9. Dorr P, Westby M, Dobbs S, Griffin P, Irvine B, Macartney M, Mori J, Rickett G, Smith-Burchnell C, Napier C, Webster R, Armour D, Price D, Stammen B, Wood A, Perros M (2005) Maraviroc (UK-427,857), a Potent, Orally Bioavailable, and

Selective Small-Molecule Inhibitor of Chemokine Receptor CCR5 with Broad-Spectrum Anti-Human Immunodeficiency Virus Type 1 Activity. Antimicrob Agents Chemother 49(11):4721–4732. doi:10.1128/aac.49.11.4721-4732.2005
10. Kola I, Landis J (2004) Can the pharmaceutical industry reduce attrition rates? Nat Rev Drug Discov 3(8):711–716
11. Niswender CM, Johnson KA, Weaver CD, Jones CK, Xiang Z, Luo Q, Rodriguez AL, Marlo JE, de Paulis T, Thompson AD, Days EL, Nalywajko T, Austin CA, Williams MB, Ayala JE, Williams R, Lindsley CW, Conn PJ (2008) Discovery, characterization, and antiparkinsonian effect of novel positive allosteric modulators of metabotropic glutamate receptor 4. Mol Pharmacol 74(5):1345–1358. doi:10.1124/mol.108.049551
12. Engers DW, Niswender CM, Weaver CD, Jadhav S, Menon UN, Zamorano R, Conn PJ, Lindsley CW, Hopkins CR (2009) Synthesis and evaluation of a series of heterobiarylamides that are centrally penetrant metabotropic glutamate receptor 4 (mGluR4) Positive Allosteric Modulators (PAMs). J Med Chem 52 (14):4115–4118. doi:10.1021/jm9005065
13. Niswender CM, Lebois EP, Luo Q, Kim K, Muchalski H, Yin H, Conn PJ, Lindsley CW (2008) Positive allosteric modulators of the metabotropic glutamate receptor subtype 4 (mGluR4): Part I. Discovery of pyrazolo[3,4-d]pyrimidines as novel mGluR4 positive allosteric modulators. Bioorg Med Chem Lett 18(20):5626–5630
14. Williams R, Niswender CM, Luo Q, Le U, Conn PJ, Lindsley CW (2009) Positive allosteric modulators of the metabotropic glutamate receptor subtype 4 (mGluR4). Part II: Challenges in hit-to-lead Bioorg Med Chem Lett 19(3):962–966
15. Williams R, Zhou Y, Niswender CM, Luo Q, Conn PJ, Lindsley CW, Hopkins CR (2010) Re-exploration of the PHCCC Scaffold: discovery of improved positive allosteric modulators of mGluR4. ACS Chem Neurosci 1(6):411–419. doi:10.1021/cn9000318
16. Todeschini R, Consonni V (2000) Handbook of Molecular Descriptors, vol 11. Methods Princ. Med Chem, Wiley - VCH
17. Hansch C, Hoekman D, Leo A, Weininger D, Selassie CD (2002) Chem-bioinformatics: comparative QSAR at the interface between chemistry and biology. Chem Rev 102(3):783–812
18. Hansch CM, Peyton P, Fujita T, Muir RM (1962) Correlation of biological activity of phenoxyacetic acids with Hammett substituent constants and partition coefficients. Nature 194:178–180
19. Cramer RD, Patterson DE, Bunce JD (1988) Comparative molecular field analysis (CoMFA). 1. Effect of shape on binding of steroids to carrier proteins. J Am Chem Soc 110(18):5959–5967. doi:10.1021/ja00226a005
20. Klebe G, Abraham U, Mietzner T (1994) Molecular Similarity Indices in a Comparative Analysis (CoMSIA) of Drug Molecules to Correlate and Predict Their Biological Activity. J Med Chem 37 (24):4130–4146. doi:10.1021/jm00050a010
21. Bleckmann A, Meiler J (2003) Epothilones: quantitative structure activity relations studied by support vector machines and artificial neural networks. QSAR Comb Sci 22(7):719–721
22. Tetko IV, Sushko I, Pandey AK, Zhu H, Tropsha A, Papa E, Oberg T, Todeschini R, Fourches D, Varnek A (2008) Critical assessment of QSAR models of environmental toxicity against Tetrahymena pyriformis: focusing on applicability domain and overfitting by variable selection. J Chem Inf Model 48(9):1733–1746
23. Winkler D (2004) Neural networks as robust tools in drug lead discovery and development. Mol Biotechnol 27(2):139–167
24. Zupan J, Gasteiger J (1993) Neural Networks for Chemists. Weinheim, VCH Verlagsgesellschaft mbH
25. Burton J, Ijjaali I, Barberan O, Petitet F, Vercauteren DP, Michel A (2006) Recursive Partitioning for the Prediction of Cytochromes P450 2D6 and 1A2 Inhibition: importance of the quality of the dataset. J Med Chem 49(21):6231–6240
26. Hecht D, Cheung M, Fogel GB (2008) QSAR using evolved neural networks for the inhibition of mutant PfDHFR by pyrimethamine derivatives. Biosystems 92(1):10–15. doi:10.1016/j.biosystems.2007.10.005
27. Hecht D, Fogel GB (2007) High-throughput ligand screening via preclustering and evolved neural networks. IEEE/ACM Trans Comput Biol Bioinform 4(3):476–484. doi:10.1109/tcbb.2007.1038
28. Butkiewicz M, Mueller R, Selic D, Dawson E, Meiler J (2009) Application of machine learning approaches on quantitative structure activity relationships. Paper presented at the IEEE Symposium on computational intelligence in bioinformatics and computational biology, Nashville
29. Mueller R, Rodriguez AL, Dawson ES, Butkiewicz M, Nguyen TT, Oleszkiewicz S, Bleckmann A, Weaver CD, Lindsley CW, Conn PJ, Meiler J (2010) Identification of metabotropic glutamate receptor subtype 5 potentiators using virtual high-throughput screening. ACS Chem Neurosci 1 (4):288–305. doi:10.1021/cn9000389
30. Schwab CH, Gasteiger J (2006) ADRIANA.Code, Algorithms for the Encoding of Molecular Structures, Version 2.0, Computerchemie MNG, Program Description
31. Niswender CM, Johnson KA, Luo Q, Ayala JE, Kim C, Conn PJ, Weaver CD (2008) A novel assay of Gi/o-Linked G protein-coupled receptor coupling to potassium channels provides new insights into the pharmacology of the group III metabotropic glutamate receptors. Mol Pharmacol 73(4):1213–1224. doi:10.1124/mol.107.041053
32. Gasteiger J, Rudolph C, Sadowski J (1990) Automatic generation of 3D atomic coordinates for organic molecules. Tetrahedron Comput Methodol 3(6c):537–547
33. Schwab CH (2007) ADRIANA.Code, 20th edn. Molecular Networks GmbH, Erlangen
34. Riedmiller M, Braun H (1992) Rprop - A Fast Adaptive Learning Algorithm. In: International Symposium on Computer and Information Science VII
35. Molecular Operating Environment (MOE) 2010.10 (2010) Chemical Computing Group Inc, 1010 Sherbooke St. West, Suite #910, Montreal, QC, Canada, H3A 2R7
36. Engers DW, Field JR, Le U, Zhou Y, Bolinger JD, Zamorano R, Blobaum AL, Jones CK, Jadhav S, Weaver CD, Conn PJ, Lindsley CW, Niswender CM, Hopkins CR (2011) Discovery, synthesis, and structure − activity relationship development of a series of N-(4-Acetamido)phenylpicolinamides as positive allosteric modulators of metabotropic glutamate receptor 4 (mGlu4) with CNS exposure in rats. J Med Chem 54(4):1106–1110. doi:10.1021/jm101271s
37. Engers DW, Gentry PR, Williams R, Bolinger JD, Weaver CD, Menon UN, Conn PJ, Lindsley CW, Niswender CM, Hopkins CR (2010) Synthesis and SAR of novel, 4-(phenylsulfamoyl)phenylacetamide mGlu4 positive allosteric modulators (PAMs) identified by functional high-throughput screening (HTS). Bioorg Med Chem Lett 20(17):5175–5178. doi:10.1016/j.bmcl.2010.07.007